BUBBLE PROPAGATION IN A FLEXIBLE-WALLED CHANNEL

A Model for the Reopening of Lung Airways

O. E. JENSEN AND M. K. HORSBURGH
Department of Applied Mathematics and Theoretical Physics, University of Cambridge, Silver Street, Cambridge CB3 9EW, UK

AND

D. P. GAVER III
Department of Biomedical Engineering, Tulane University, New Orleans, LA 70118-5674, USA

1. Introduction

The airways of the lung form a network of bifurcating flexible tubes that are lined on their interior with a layer of viscous liquid. Surface tension acting at the air-liquid interface therefore plays a major role in the mechanics of respiration [4]. Capillary instabilities, for example, can redistribute the liquid lining of airways to form lenses or lamellae that occlude the airway. Surface tension can also cause direct occlusion of small airways, by exerting compressive stresses that cause airway walls to collapse. A consequence of elevated levels of surface tension is therefore a high incidence of collapsed, flooded airways, leading to impaired gas exchange. This is one of the more serious difficulties faced by premature infants suffering Respiratory Distress Syndrome (RDS), a condition associated with their inability to produce adequate quantities of pulmonary surfactant.

To reopen a collapsed airway, and to restore gas exchange, a bubble of air must be blown along the airway so that the airway walls can be peeled apart and then held open. For a premature infant with RDS, this bubble might be driven by spontaneous breathing or by imposed ventilation. Airway walls are delicate structures that are easily damaged by excessive stresses, so that a model predicting the forces exerted on an airway during reopening is an important tool in developing clinical ventilation strategies. Other instances where it is valuable to have an understanding of the effort

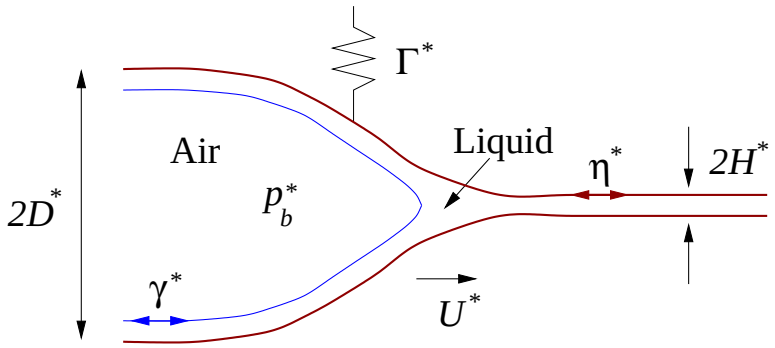

Figure 1. The model problem: a semi-infinite bubble is blown into a liquid-filled channel. The advancing bubble peels apart the channel walls, compressing external springs.

required to reopen a collapsed airway include asthma (when the smooth muscle surrounding an airway is in spasm), cystic fibrosis (when the liquid lining is excessively viscous) and obstructive sleep apnea (when the walls of upper airways have poor muscle tone).

The airway reopening problem has motivated a number of investigations of model systems such as that illustrated in figure 1. A semi-infinite bubble held at uniform pressure p_b^* advances steadily at speed U^* into a liquid-filled channel. The channel's walls are formed by two inextensible membranes that are supported by external springs with stiffness Γ^* and that are held under longitudinal tension η^*; far ahead of the bubble the channel has width $2H^*$, the fluid is at rest relative to the walls and the springs are unstressed. The air-liquid interface is assumed to have uniform surface tension γ^* and the liquid has constant viscosity μ^*. The effects of membrane damping, inertia and gravity are assumed negligible, as are variations in longitudinal tension due to viscous stresses acting on the membranes. The relationship between p_b^* and U^* is sought as a function of the remaining material parameters. The motion is assumed to be planar and symmetric about the channel's midline.

Experiments using this and closely related physical systems have revealed the following behaviour [3, 11, 12]: (i) for a given experimental configuration, data obtained for many values of μ^*, γ^*, H^*, Γ^* and η^* collapse quite closely onto a single curve if $p_b^* D^*/\gamma^*$ is plotted against $Ca = \mu^* U^*/\gamma^*$, where $2D^*$ is the width of the inflated channel (see figure 1); (ii) steadily propagating bubble motion is achievable only for $p_b^* D^*/\gamma^*$ in excess of a critical 'yield' pressure; (iii) for pressures in excess of this threshold, bubble speed is a monotonically increasing function of bubble pressure.

A theoretical study of the model system shown in figure 1, undertaken

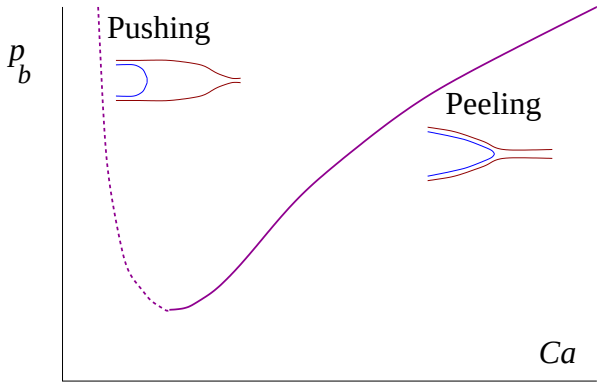

Figure 2. Steady solutions of the model reopening problem, shown schematically. Inserts show the characteristic membrane and bubble shapes for 'pushing' and 'peeling' motions.

by Gaver *et al.* [2], captured many of these experimental observations. In this study, lengths were scaled on H^*, speeds on U^* and pressure on γ^*/H^*, so that the problem was governed by the nondimensional parameters

$$p_b = \frac{p_b^* H^*}{\gamma^*}, \quad Ca = \frac{\mu^* U^*}{\gamma^*}, \quad \Gamma = \frac{\Gamma^* H^{*2}}{\gamma^*} \quad \text{and} \quad \eta = \frac{\eta^*}{\gamma^*}. \tag{1}$$

The relationship between bubble pressure p_b and bubble speed Ca (a capillary number) was sought in terms of the membrane's elastic properties, represented by a dimensionless spring constant Γ and membrane tension η. Numerical simulations were undertaken using a boundary element method (BEM) to compute the steady Stokes flow in the channel; the numerical solution domain was extended by using lubrication theory to describe the flow far upstream and downstream of the bubble tip. The results of these computations are summarized in figure 2; numerical results are shown in figure 5 below.

For given η and Γ, two steady solution branches were found. At small Ca, a solution branch exists for which p_b is a diminishing function of Ca. In this case the channel is widely inflated over a long region ahead of the bubble, and the bubble appears to 'push' ahead of itself a long column of liquid (as sketched in figure 2). An asymptotic analysis in the limit $Ca \ll 1$, based on the theory of Bretherton [1], indicates that $p_b \propto \Gamma Ca^{-2/3}$ as $Ca \to 0$. This behaviour is contrary to experimental observations that p_b increases with Ca, and this solution branch was postulated in [2] to be unstable to disturbances at constant p_b. A second solution branch exists for sufficiently large p_b and Ca, for which p_b increases with Ca. This is consistent with experimental observation and this solution branch was therefore presumed to be stable to perturbations at constant p_b. Motion on the right-hand

branch may be characterised as 'peeling' apart of the channel walls by the advancing bubble, reminiscent of the peeling motion of an adhesive strip pulled from a surface described by McEwan & Taylor [9].

Recently, we showed [6] how this peeling motion may be captured using an asymptotic model that is not subject to the usual condition $Ca \ll 1$, but instead requires that the membrane tension η is large, so that the capillary number based on membrane tension is small ($Ca/\eta = \mu^* U^*/\eta^* \ll 1$), while the capillary number based on surface tension ($Ca = \mu^* U^*/\gamma^*$) is $O(1)$. In this limit the membrane slope is everywhere small, so that near the bubble tip the channel walls are locally flat and almost parallel; the local two-dimensional Stokes flow is then equivalent at leading order to the canonical problem of a semi-infinite bubble advancing into a parallel-sided channel. Numerical solutions of this problem [5, 13, 14, 15] provide key quantities that enter boundary conditions for a long-wavelength description of the remainder of the flow. Such an approach was successfully taken by Ruschak in describing roll coating flows [15], was used semi-empirically by McEwan & Taylor [9], and it is equally powerful in describing the reopening problem. A brief outline of the approach is provided below; for full details see [2, 6].

2. The asymptotic model

We first define the following two parameters in terms of those in (1):

$$\epsilon \equiv \left(\frac{Ca}{\eta}\right)^{1/3} = \left(\frac{\mu^* U^*}{\eta^*}\right)^{1/3}; \quad \delta \equiv \left(\frac{\Gamma^3}{\eta\ Ca^2}\right)^{1/6} = \left(\frac{\Gamma^{*3} H^{*6}}{\eta^* \mu^{*2} U^{*2}}\right)^{1/6}. \quad (2)$$

We consider here the limit of large membrane tension ($\eta \gg 1$, a condition common to all previous experiments and computations), and so we assume primarily that $\epsilon \ll 1$ (requiring $Ca \ll \eta$), but we allow δ to remain $O(1)$. The analysis simplifies in the special case $\delta \ll 1$, which then restricts Ca to the range $(\Gamma^3/\eta)^{1/2} \ll Ca \ll \eta$.

When $\epsilon \ll 1$, the flow can be split into three distinct asymptotic domains, as illustrated in figure 3: a wall-statics region (region I), in which the membrane is in equilibrium and the liquid layer sits passively on the membrane; a Stokes flow region at the bubble tip (region II); and a slender region ahead of the bubble tip (region III) in which there is typically a dominant balance between viscous forces and membrane tension. Working in the frame of the bubble tip, there is a unit volume flux of liquid from right to left in figure 3 throughout each region. The membrane lies along $y = h(x)$, and the bubble tip lies at $x = 0$, $y = 0$. We will show briefly how this system may be reduced to a third-order nonlinear eigenvalue problem for p_b when $\epsilon \ll 1$, $\delta = O(1)$ ((8–11) below), which simplifies further to yield an explicit formula for p_b ((13) below) when $\epsilon \ll 1$ and $\delta \ll 1$.

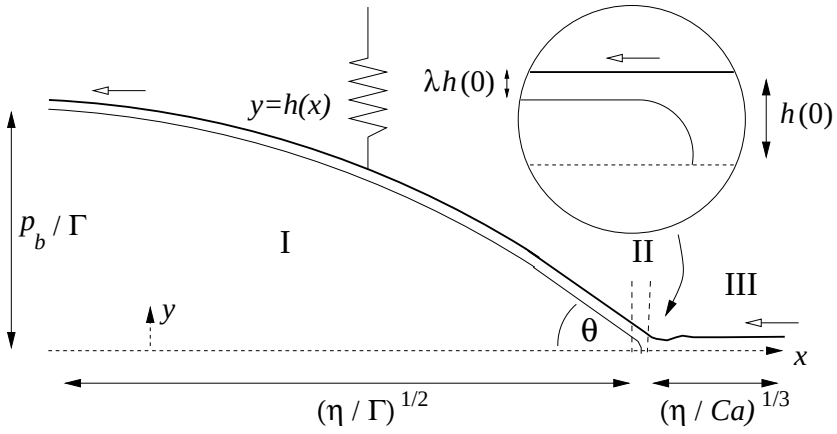

Figure 3. In the frame of the bubble tip, the channel wall at $y = h(x)$ moves from right to left with unit speed. The bubble lies in $x < 0$. The horizontal dotted line (the x-axis) is a line of symmetry. The inset shows the structure of the inner region II.

2.1. REGION I

Here the channel is inflated by the bubble pressure p_b; the pressure outside the channel is taken to be zero. Since $\eta \gg 1$, membrane tension dominates the effects of surface tension, and so the membrane shape is controlled at leading order by a normal stress balance

$$p_b = \Gamma(h - 1) - \eta h_{xx}. \tag{3}$$

The maximum channel width D^*/H^* is $O(p_b/\Gamma)$, controlled by the external springs, while the lengthscale of region I is $O((\eta/\Gamma)^{1/2})$, controlled by a balance between the springs and membrane tension. It follows that the small peeling angle near the bubble tip (see figure 3) $\theta = O(p_b/(\eta\Gamma)^{1/2})$.

2.2. REGION II

The flow near the bubble tip over lengthscales comparable to the local channel width $h(0)$ (see the inset on figure 3) may be shown [6] to be equivalent at leading order in ϵ to the two-dimensional Stokes-flow problem for an advancing semi-infinite bubble in a planar channel. Numerical solutions of this canonical problem over a wide range of Ca [5, 13–15] provide estimates of $\lambda(Ca)$ (the thickness of the deposited film behind the advancing bubble relative to channel half-width), and $\mathcal{P}(Ca)$, the net pressure drop across the bubble tip. Since there is unit volume flux through region II,

$$\lambda h(0) = 1. \tag{4}$$

The pressure a few channel widths ahead of the meniscus is uniform across the channel and has the distribution

$$p \sim p_b - 3x\,Ca\,(1-\lambda)[h(0)]^{-2} + Ca\,\mathcal{P}[h(0)]^{-1} + \ldots \tag{5}$$

In the limit $Ca \to 0$, $\lambda \sim 1.337\,Ca^{2/3}$ and $Ca\,\mathcal{P} \sim -1.0 - 3.80\,Ca^{2/3}$ [1, 10, 14], but these asymptotic predictions are poor approximations if Ca is not small. Instead we use numerically-determined regression formulae for λ and $\mathcal{P}$ (given in the Appendix) that are valid for a wide range of Ca.

2.3. REGION III

Far ahead of the bubble tip the channel is slender and lubrication theory may be applied, which yields the following expression for the volume flux:

$$1 = \frac{h^3}{3\,Ca}\,p_x + h \quad \text{where} \quad p = \Gamma(h-1) - \eta h_{xx}, \tag{6}$$

with $h \to 1$ as $x \to \infty$. When the springs are weak ($\delta \ll 1$), membrane tension and viscous forces are dominant, and the lengthscale over which the channel width $h(x)$ varies in region III is therefore of order $(\eta/Ca)^{1/3} = \epsilon^{-1}$, so the peeling angle at the bubble tip $\theta = O(\epsilon)$.

2.4. MATCHING

Combining the estimates of θ from regions I and III above gives a leading-order estimate of bubble pressure

$$p_b \sim \beta\Gamma^{\frac{1}{2}}\eta^{\frac{1}{6}}\,Ca^{\frac{1}{3}} \equiv \beta\Gamma/\delta \qquad \text{when} \qquad \epsilon \ll 1, \quad \delta \ll 1, \tag{7}$$

for some $O(1)$ quantity β (which turns out to depend weakly on Ca). In terms of dimensional variables, with p_b^* scaled with the half-width D^* of the inflated channel, $p_b^*/(\gamma^*/D^*) \sim \beta^2\eta^{1/3}\,Ca^{2/3}$, which is independent of H^* and Γ^*, only weakly dependent on membrane tension and an increasing function of Ca, as observed experimentally [3, 11, 12].

If we set $p_b = (\Gamma/\delta)P_b$ (given (7)) and $X = \epsilon x$, (6) becomes

$$\tfrac{1}{3}h^3(h_{XXX} - \delta^2 h_X) = h - 1, \qquad h \to 1 \quad \text{as} \quad X \to \infty, \tag{8}$$

in $X \geq 0$. Taking $\epsilon \ll 1$ and $\delta = O(1)$, formal matching across region II yields boundary conditions for (8)

$$h(0) = \lambda^{-1}, \tag{9}$$

$$h_X(0) = -P_b + \delta\left(\lambda^{-1} - 1\right), \tag{10}$$

$$h_{XX}(0) = -\epsilon\mathcal{P}\lambda - \delta P_b + \delta^2\left(\lambda^{-1} - 1\right), \tag{11}$$

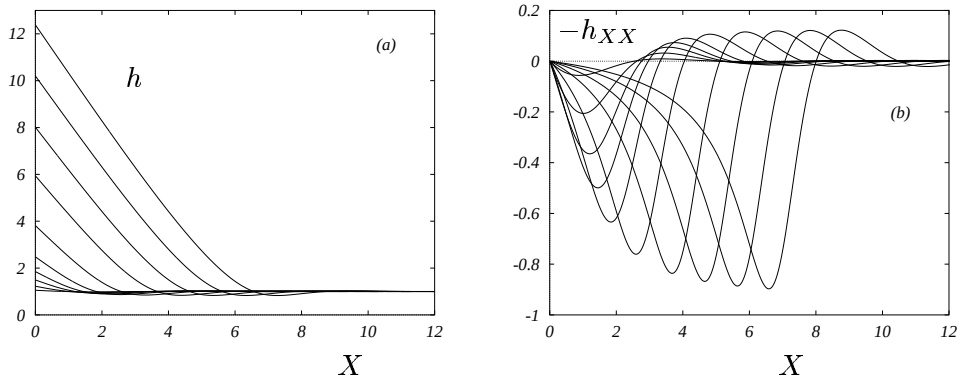

Figure 4. (*a*) Solutions of (12) for which $h_{XX}(0) = 0$: (*b*) shows the corresponding values of $-h_{XX}(X)$ (proportional to the pressure).

which ensure continuity of volume flux (from 4), peeling angle and pressure (from 5) respectively.

Linearisation about $h = 1$ shows that there is a two-parameter family of solutions of (8) that decay as $X \to \infty$. With three additional conditions (9–11), (8–11) represents a nonlinear eigenvalue problem for P_b, dependent on the three parameters (Γ, η, Ca). This was solved in [6] using finite differences and Newton's method; results are presented below.

2.5. PEELING MOTION

A simplified problem emerges when $\epsilon \ll 1$ and $\delta \ll 1$. In this limit the springs are weak, so that the channel is inflated to a width that is much wider than the collapsed channel ahead of the bubble tip, corresponding to a peeling motion. A double expansion in powers of ϵ and δ of (8–11) reduces at leading order to the Landau–Levich equation [7]

$$\tfrac{1}{3}h^3 h_{XXX} = h - 1, \qquad h \to 1 \quad \text{as} \quad X \to \infty, \tag{12}$$

subject to $h(0) = 1/\lambda(Ca)$, $h_X(0) = -P_b$, $h_{XX}(0) = 0$. There is a one-parameter family of solutions of (12) for which $h_{XX}(0) = 0$, shown in figure $4(a, b)$. At this order in δ, the pressure in the liquid ahead of the bubble tip is an order of magnitude larger than the bubble pressure. Once Ca is specified, then $h(0)$ is fixed and the eigenvalue problem dictates the slope $h_X(0) = -\beta(Ca)$, say. This function is well approximated by a regression formula given in the Appendix. Then $P_b = \beta(Ca) + O(\epsilon, \delta)$, as in (7).

The $O(\epsilon, \delta)$ corrections to this estimate of P_b were computed in [6] by perturbing this leading-order solution, leading to the following explicit

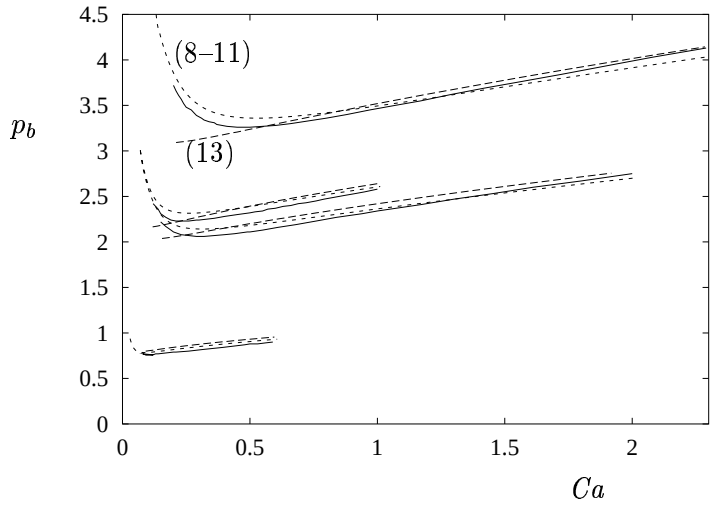

Figure 5. BEM results (solid) from figure 14 of [2] are compared with asymptotic predictions obtained using the formula (13) (long dashes) and numerically using (8–11) (short dashes) for, from top to bottom, $(\Gamma, \eta) = (1, 100)$, $(0.5, 250)$, $(0.5, 100)$, $(0.1, 100)$.

prediction for p_b in terms of Ca,

$$p_b \approx \beta \Gamma^{\frac{1}{2}} \eta^{\frac{1}{6}} Ca^{\frac{1}{3}} + \Gamma \left[\lambda^{-1} - 1 + \chi\beta \right] + \Gamma^{\frac{1}{2}} \eta^{-\frac{1}{6}} Ca^{\frac{2}{3}} \chi \lambda \mathcal{P}, \qquad (13)$$

which is supplemented with regression formulae for $\lambda(Ca)$, $\mathcal{P}(Ca)$, $\beta(Ca)$ and $\chi(Ca) \equiv \frac{1}{3} \left[\beta/(\lambda^2 - \lambda^3) \right] \mathrm{d}h_{0X}(0)/\mathrm{d}h_0(0)$ given in the Appendix.

3. Results

The accuracy of the asymptotic predictions can be demonstrated by testing them against full numerical (BEM) solutions of the model reopening problem obtained in [2]. Figure 5 shows the BEM solutions (solid lines) compared with (i) predictions of p_b obtained by solving the nonlinear eigenvalue problem (8–11), which assumes $\epsilon \ll 1$, and (ii) the explicit formula (13) which assumes $\epsilon \ll 1$ and $\delta \ll 1$. Equation (13) captures the right-branch behaviour well for this range of Ca, but fails to describe the turning point in the p_b–Ca relationship, since δ increases as Ca falls. However the nonlinear eigenvalue problem (8–11) accurately captures both solution branches, and therefore provides a relatively simple way of computing the yield pressure above which steady reopening is possible.

Further comparisons were also conducted in [6] for the asymmetric flow configuration used in [11], for which the channel has one rigid wall and one deformable wall. In this case BEM predictions of p_b in [6] compare

closely with experimental results [11] over an extensive range of Ca. In contrast, the corresponding asymptotic theory captures the solution branch near the turning point well (much as in figure 5), but underestimates the experimental data and BEM results once Ca increases above about 1.5; this disagreement arises because for these values of Ca the small-slope parameter ϵ increases above about 0.3 (for the corresponding values of Γ and η).

4. Discussion

The asymptotic model summarized here, and presented in detail in [6], provides a powerful and robust tool for investigating a range of reopening problems. It has been validated against experiment and two independent sets of BEM data, and has been shown to be quantitatively accurate as long as the membrane slope is sufficiently small. It demonstrates explicitly how the Stokes flow in the neighbourhood of the bubble tip acts as a valve, so that the flux of liquid permitted to squeeze past the bubble tip depends on the bubble speed. This short quasi-steady 'inner' region therefore controls the dynamics of reopening. We have recently extended the model to include unsteady effects to verify the postulated stability properties of the two solution branches in figure 2, and we are using it to investigate the large transient stresses that develop during the initiation of reopening [11]; details will be presented elsewhere. When $\epsilon \ll 1$, $\delta \ll 1$, the model predicts the leading-order peeling angle to be

$$\theta(Ca) \approx \beta(Ca)(Ca/\eta)^{\frac{1}{3}}, \tag{14}$$

(see figure 3), where β is an $O(1)$ function given in the Appendix; this can be regarded as an analogue of Tanner's law relating the apparent contact angle of a spreading drop to the speed of an advancing contact line [8]. The model also shows that the dominant resistance to steady reopening is provided by the very low pressures in the liquid ahead of the bubble tip, arising because of large membrane tension. The most harmful stresses exerted on an airway wall may therefore be inward normal stresses that are substantially greater in magnitude than p_b.

Numerous aspects of real airway mechanics have been neglected in this simple model. Fingering instabilities were a prominent feature of the peeling motions described by McEwan & Taylor [9], and are likely to be present in experiments (and possibly airways) at sufficiently large Ca, although direct experimental observations are scarce [3]. Elastic-walled tubes buckle to a complex non-axisymmetic configuration when collapsed, and so the planar models described above give at most a qualitative picture of the motion of a fully three-dimensional dynamic reopening problem. Surfactants undoubtedly have a significant effect in pulmonary applications; a recent study for

soluble surfactants at low bulk Péclet numbers [16] provides an important first step in this direction.

Appendix

The regression formulae used in the asymptotic model are as follows:
$\lambda(Ca) \approx 0.417\left(1-\exp\left[-1.69\,Ca^{0.5025}\right]\right)$ from [5];
$\log_{10}(-\mathcal{P}) \approx -2.00858+8.92426\,\exp\left[-0.038332\,(Z+5)^{2.17398}\right]+0.898217\,Z$
where $Z \equiv \log_{10} Ca$ for $10^{-2} \leq Ca \leq 10$;
$\beta(Ca) \approx 0.988113+(0.366815-0.184297\,z)\exp\left(-0.000159689\,(z+8)^{4.08538}\right)$
and
$\chi(Ca) \approx 0.234261 - 1.63071\,\exp(-0.3487\,z) - 0.368093\,z + 0.0279832\,z^2$
where $z \equiv \log Ca$ for $-4 \leq \log Ca \leq 4$.

References

1. Bretherton, F.P. (1961) The motion of long bubbles in tubes. *J. Fluid Mech.* **10**, 166–188.
2. Gaver, D.P. III, Halpern, D., Jensen, O.E. & Grotberg, J.B. (1996) The steady motion of a semi-infinite bubble through a flexible-walled channel. *J. Fluid Mech.* **319**, 25–65.
3. Gaver, D.P. III, Samsel, R.W. & Solway, J. (1990) Effects of surface tension and viscosity on airway reopening. *J. Appl. Physiol.* **69**, 74–85.
4. Grotberg, J.B. (1994) Pulmonary flow and transport phenomena. *Ann. Rev. Fluid Mech.* **26**, 529–571.
5. Halpern D. & Gaver, D.P. III (1994) Boundary-element analysis of the time-dependent motion of a semi-infinite bubble in a channel. *J. Comp. Phys.* **115**, 366–375.
6. Jensen, O.E., Horsburgh, M.K. & Gaver, D.P. III (1999) The steady propagation of a bubble in a flexible-walled channel: asymptotic and computational methods. *Phys. Fluids (submitted).*
7. Landau, L. & Levich, B. (1942) Dragging of a liquid by a moving plate. *Acta Physchim. URSS* **17**, (1–2), 42–54.
8. Leger, L. & Joanny, J.F. (1992) Liquid spreading. *Rep. Prog. Phys.* **55**, 431–486.
9. McEwan, A.D. & Taylor, G.I. (1966) The peeling of a flexible strip attached by a viscous adhesive. *J. Fluid Mech.* **26**, 1–15.
10. Park, C.W. & Homsy, G.M. (1984) Two-phase displacement in Hele Shaw cells: theory. *J. Fluid Mech.* **139**, 291–308.
11. Perun, M.L. & Gaver, D.P III (1995) An experimental model investigation of the opening of a collapsed untethered pulmonary airway. *J. Biomech. Eng.* **117**, 245–253.
12. Perun, M.L. & Gaver, D.P III (1995) Ineraction between airway lining fluid forces and parenchymal tethering during pulmonary airway reopening. *J. Appl. Physiol.* **79**, 1717–1728.
13. Reinelt, D.A. (1987) Interface conditions for two-phase displacement in Hele-Shaw cells. *J. Fluid Mech.* **183**, 219–234.
14. Reinelt, D.A. & Saffman, P.G. (1985) The penetration of a finger into a viscous fluiid in a channel and tube. *SIAM J. Sci. Stat. Comput.* **6**, 542–561.
15. Ruschak, K.J. (1982) Boundary-conditions at a liquid-air interface in lubrication flows *J. Fluid Mech.* **119**, 107–120.
16. Yap, D.Y.K. & Gaver, D.P. III (1998) The influence of surfactant on two-phase flow in a flexible-walled channel under bulk equilibrium conditions. *Phys. Fluids* **10**, 1846–1863.